Available online at www.sciencedirect.com
SCIENCE DIRECT®
Journal of Power Sources 134 (2004) 293–297
JOURNAL OF POWER SOURCES
www.elsevier.com/locate/jpowsour

Li_2CO_3 in $LiNi_{0.8}Co_{0.15}Al_{0.05}O_2$ cathodes and its effects on capacity and power

Guorong V. Zhuang [a], Guoying Chen [b], Joongpyo Shim [b], Xiangyun Song [b], Philip N. Ross [a], Thomas J. Richardson [b,*]

[a] *Materials Sciences Division, Ernest Orlando Lawrence Berkeley National Laboratory, Berkeley, CA 94720, USA*
[b] *Environmental Energy Technologies Division, Ernest Orlando Lawrence Berkeley National Laboratory, Berkeley, CA 94720, USA*

Received 4 February 2004; accepted 28 February 2004

Available online 15 June 2004

Abstract

Lithium carbonate is commonly found on the surfaces of lithiated cathode active materials that have been exposed to air. Long-term exposure of $LiNi_{0.8}Co_{0.15}Al_{0.05}O_2$ electrodes produced a dense Li_2CO_3 coating, approximately 10 nm in thickness that severely reduced both the accessible capacity and the rate at which the electrodes could be cycled. Ex situ X-ray diffraction patterns of cycled electrodes revealed a bimodal distribution of active material in different states of charge. Particle isolation is proposed to contribute to both capacity and power losses, and possible mechanisms related to the formation of Li_2CO_3 are discussed.

Keywords: Lithium batteries; Battery power; Battery capacity; Power fade; Capacity fade

1. Introduction

The presence of lithium carbonate on the surfaces of active cathode materials such as $LiNiO_2$ and its analogues $LiNi_{1-x-y}Co_xAl_yO_2$ has long been noted [1–10]. Matsumoto et al. carried out a detailed study [6] of the reaction of $LiNi_{1-x-y}Co_xAl_yO_2$ with CO_2 and concluded that the rate of reaction was limited by diffusion of CO_2 through a dense surface layer of Li_2CO_3. The formation of Li_2CO_3 is presumed to take place via reaction (1).

$$LiNi_{0.8}Co_{0.15}Al_{0.05}O_2 + \tfrac{1}{4}xO_2 + \tfrac{1}{2}xCO_2 \Rightarrow Li_{1-x}Ni_{0.8}Co_{0.15}Al_{0.05}O_2 + \tfrac{1}{2}xLi_2CO_3 \quad (1)$$

While some correlations between electrochemical properties and Li_2CO_3 contamination have been demonstrated, no detailed study has specifically addressed the issue of capacity and power losses that result from its presence in electrodes. Here we show that air exposure of $LiNi_{0.8}Co_{0.15}Al_{0.05}O_2$ cathodes fabricated for use in high-power cells may produce a large amount of Li_2CO_3 that severely limits the performance of the electrodes by means of partial or complete isolation of active material.

2. Experimental

The $LiNi_{0.8}Co_{0.15}Al_{0.05}O_2$ cathode laminates, obtained from the USDOE Advanced Technology Development Program [11], contained 84 wt.% $LiNi_{0.8}Co_{0.15}Al_{0.05}O_2$ powder (Fuji CA1505), 4 wt.% amorphous carbon (Chevron), 4 wt.% graphite (SFG-6, Timcal) and 8 wt.% polyvinylidene difluoride (PVDF) binder (Kureha KF-1100). The "air-exposed" electrodes had been stored in an open envelope for a period of about 2 years. Fresh, new electrodes were prepared for comparison from identical active material that had been stored in a dry, airtight container. Swagelok®-type cells using 1.6 cm^2 cathodes, Li counter electrodes, Celgard 3401 polypropylene separators and 1 M $LiPF_6$ in 1:1 ethylene carbonate:propylene carbonate (Ferro Corporation) were assembled in a He-filled glove box (O_2 < 1 ppm, H_2O < 5 ppm). Galvanostatic cycling tests were performed in sealed cells at ambient temperature. Cathodes were removed from the cycled cells and washed with dry dimethylcarbonate in the glovebox to remove electrolyte residues.

FT-IR measurements were performed using a Nicolet Nexus 870 spectrometer, equipped with a broadband mercury–cadmium–telluride (MCT) detector. The spectra were acquired in the highly surface-sensitive attenuated total reflection (ATR) mode with a spectral resolution of

* Corresponding author. Tel.: +1-510-486-8619; fax: +1-510-486-8619.
E-mail address: tjrichardson@lbl.gov (T.J. Richardson).

0378-7753/$ – see front matter © 2004 Elsevier B.V. All rights reserved.
doi:10.1016/j.jpowsour.2004.02.030

4 cm^{-1}. The ATR-FT-IR spectra were corrected for the light penetration depth (~0.4 μm) as function of wavelength. A linear background correction was also performed to eliminate the sloping spectral background caused by surface roughness. The vibrational modes of $LiNi_{0.8}Co_{0.15}Al_{0.05}O_2$ are outside the spectral region measured (4000–700 cm^{-1}). Transmission electron microscopy (TEM) was carried out using a Philips CM200 microscope with energy dispersive X-ray analysis (EDX). Samples were scraped from electrodes, washed with dimethyl carbonate, and mounted on carbon grids in the glove box. X-ray diffraction (XRD) patterns were acquired in reflection mode using a Panalytical Xpert Pro diffractometer with monochromatized Cu Kα radiation. The scan rate was 0.001° s^{-1} from 15° to 70° 2θ in 0.01° steps. Lattice parameters, state of charge, and compositions were determined by whole pattern refinement using the program RIQAS (MDI Inc.).

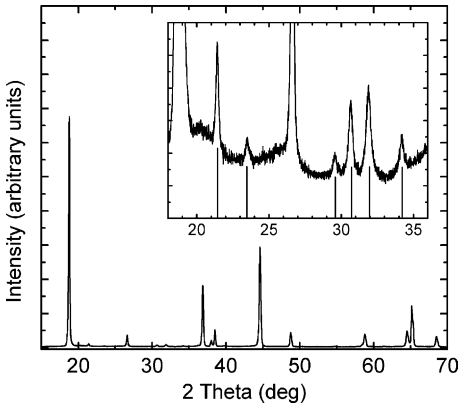

Fig. 2. XRD pattern of air-exposed $Li_xNi_{0.8}Co_{0.15}Al_{0.05}O_2$ electrode. Locations of diffraction peaks due to Li_2CO_3 are marked in the inset plot. The peaks at 18.7° and 26.5° are (0 0 3) for the active material and (0 0 2) for graphite, respectively.

3. Results and discussion

3.1. Li_2CO_3 in air-exposed powder and electrodes

The ATR-FT-IR spectrum (Fig. 1, curve a) of $LiNi_{0.8}Co_{0.15}Al_{0.05}O_2$ powder that had been stored in a sealed container until just before the measurement consists entirely of absorptions due to Li_2CO_3, although no evidence for Li_2CO_3 contamination was found in XRD measurements (detection limit ca. 0.1%). The strong peak at 1422 cm^{-1} and shoulder at 1479 cm^{-1} are the C–O asymmetric and symmetric stretching modes of Li_2CO_3, while the CO_3 group bending mode gives rise to a sharp peak at 870 cm^{-1}. The discrepancy between ATR-FT-IR and XRD can be attributed to the fact that the FT-IR technique has high surface sensitivity and is largely unaffected by crystallite size. In the spectra of the cathodes (Fig. 1, curves b and c), the region between 1300 and 880 cm^{-1} is dominated by absorptions due to the PVDF binder. The strongest peak (1174 cm^{-1}) is attributed to CF_2 asymmetric stretching mode in PVDF.

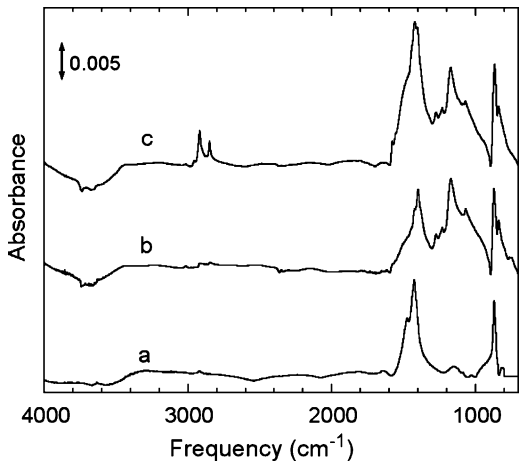

Fig. 1. FT-IR spectra of (a) $LiNi_{0.8}Co_{0.15}Al_{0.05}O_2$ powder, (b) surface of fresh cathode, and (c) surface of air-exposed cathode.

Although the Li_2CO_3 content in electrodes is difficult to quantify by ATR-FT-IR, by comparing the peak intensity ratios at 1422 and 1174 cm^{-1} (Fig. 1, curves b and c), which are characteristic of the carbonate group and CF_2 group in PVDF, respectively, it was estimated that the old, air-exposed electrode contained about twice as much Li_2CO_3 as the fresh one. It has been reported that Li_2CO_3 disappears from FT-IR spectra [12] of $LiCoO_2$ and $LiMn_2O_4$ electrodes and from X-ray photoelectron spectra [8] of $LiNi_{0.8}Co_{0.2}O_2$ cathode surfaces after cycling. Recently, we observed similar behavior in lightly contaminated $LiNi_{0.8}Co_{0.15}Al_{0.05}O_2$ electrodes stored or cycled in $LiPF_6$ EC/DEC (1:1) electrolyte [13].

Li_2CO_3 in the freshly prepared electrode as determined by XRD was about 0.5 wt.% of the oxides present, while the electrode exposed to air for 2 years contained more than 6 wt.% Li_2CO_3 (Fig. 2). The latter was well crystallized (average crystallite size: 50 nm). Since the lattice parameters of $Li_{1-x}Ni_{0.8}Co_{0.15}Al_{0.05}O_2$ vary in an approximately linear fashion with x [14], these were used to make a rough estimate of the state of charge of materials in electrodes and powder samples. The active material in the long-exposed electrode was significantly oxidized (Table 1). If all of the lithium carbonate found in this electrode had been produced by extraction according to reaction (1), the active material would have $x \approx 0.16$. This is about twice the value estimated from the change in lattice parameters. Some excess lithium may be present in the raw powder in the form of Li_2O or LiOH, which are not easily detected by XRD. Exposure to atmospheric moisture and CO_2 may convert this synthetic residue to crystalline Li_2CO_3. This would also help to account for the very rapid appearance of Li_2CO_3 on the surfaces of fresh samples following brief exposure to air.

A high-resolution transmission electron micrograph of fresh $LiNi_{0.8}Co_{0.15}Al_{0.05}O_2$ powder (Fig. 3a) shows good crystallinity at the edges of the grains and no evidence

Table 1
Cell parameters and approximate state of charge from XRD analysis

Sample	Li_2CO_3 (wt.%)	a_0 (Å)	c_0 (Å)	x_{XRD}	mol %[a]
Fresh powder	0.0	2.863	14.178	0.00	100
Fresh electrode	0.5	2.861	14.184	0.02	100
Fresh electrode	0.5	2.842	14.248	0.12	70
charged		2.857	14.182	0.03	30
Air-exposed electrode	6.1	2.862	14.226	0.07	100
Air-exposed electrode	3.0	2.836	14.358	0.29	57
after charging		2.862	14.212	0.05	43
Air-exposed electrode	3.0	2.839	14.339	0.26	59
after 7 days		2.861	14.213	0.06	41

[a] Active components only.

for a surface film. By contrast, oxide particles from the air-exposed cathode (Fig. 3b) are covered by an apparently continuous layer at least 10 nm thick. Elemental analysis by EDX showed the coating to be composed primarily of carbon and oxygen, consistent with its identification as lithium carbonate by FT-IR and XRD. The surface area of the active material is 0.4 $m^2\,g^{-1}$, and the porosity of the electrode is about 38%. A uniform coating of 6 wt.% Li_2CO_3 on all surfaces of the active particles would be roughly 75 nm thick and would occupy about 1/6 of the pore volume, assuming no volume expansion of the cathode composite due to Li_2CO_3 formation. The fact that the observed coating is thinner than predicted supports the notion that not all of the Li_2CO_3 present was formed by extraction from the layered oxide.

3.2. Electrochemical performance

Charge and discharge potential profiles for cells made from fresh and air-exposed cathodes are presented in Fig. 4. The cells were cycled five times at the lowest rate ("*C*" is the discharge capacity at this rate) and then the rates were gradually increased. The capacity of the heavily contaminated electrode cathode was much lower at all rates than that of the fresh cathode. Even at very low rates, the highly contaminated electrode delivered less than half the capacity of the fresh one. Both cells exhibited high resistance on the first charge, requiring extended charging at a reduced current, i.e. taper charging, at 4.1 V. On discharge, nearly all of the first charge capacity was recovered. The decrease in resistance following this first charge may reflect some dissolution or electrolyte penetration of the carbonate coating, possibly due to production of acid species during charging or to dimensional changes in the underlying particles. Even after extended cycling and following overcharging to 4.3 V, however, more than half the initial Li_2CO_3 was still present in the heavily contaminated electrode.

3.3. Ex situ XRD

A fresh electrode was charged as rapidly as possible without damaging it by polarizing the cell at 4.1 V for 1.6 h until a total charge of 280 $\mu Ah\,cm^{-2}$, corresponding to $x = 0.12$, had been passed. The cell was disassembled within a minute and the electrode was washed thoroughly with dimethyl carbonate and vacuum dried before removal from the glove box. Fitting of the entire pattern was carried out to obtain the cell parameters. For simplicity, only the $LiNi_{0.8}Co_{0.15}Al_{0.05}O_2$ 003 peak profiles for the fresh and charged electrode are shown in Fig. 5. The active material in the fresh electrode is single-phase and in the fully discharged state (Table 1). Because the material expands in the direction of the *c*-axis as it

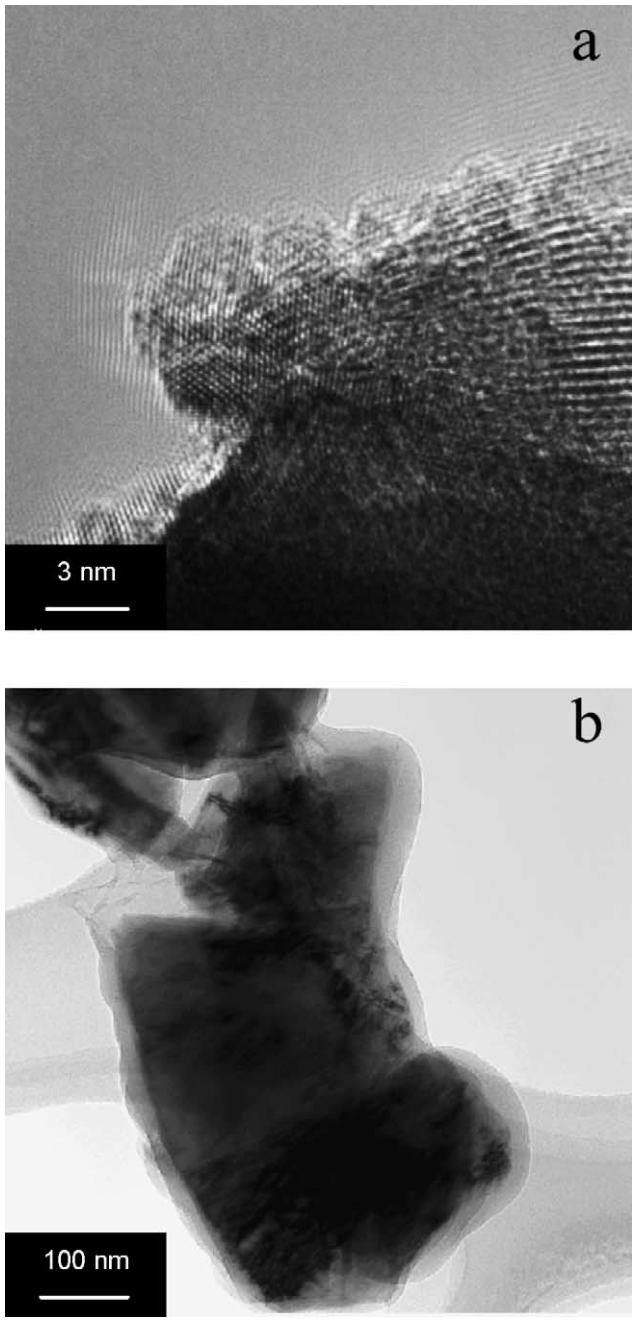

Fig. 3. TEM images of (a) fresh $Li_xNi_{0.8}Co_{0.15}Al_{0.05}O_2$ powder and (b) $Li_xNi_{0.8}Co_{0.15}Al_{0.05}O_2$ grain from air-exposed electrode.

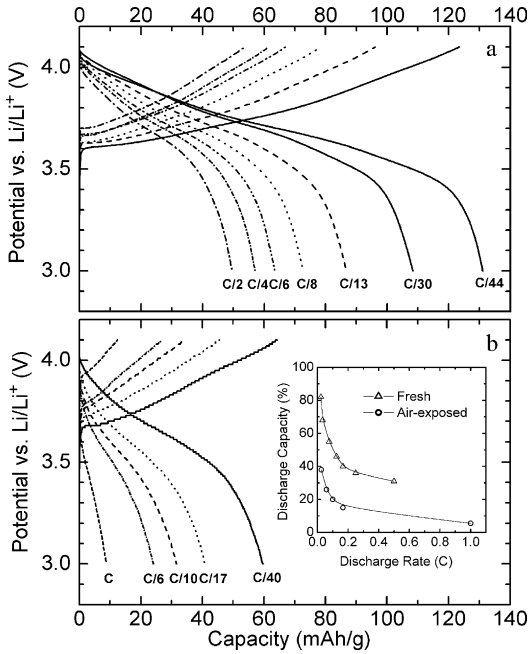

Fig. 4. Charge and discharge profiles for (a) fresh cathode and (b) air-exposed cathode. Inset: discharge capacity vs. rate.

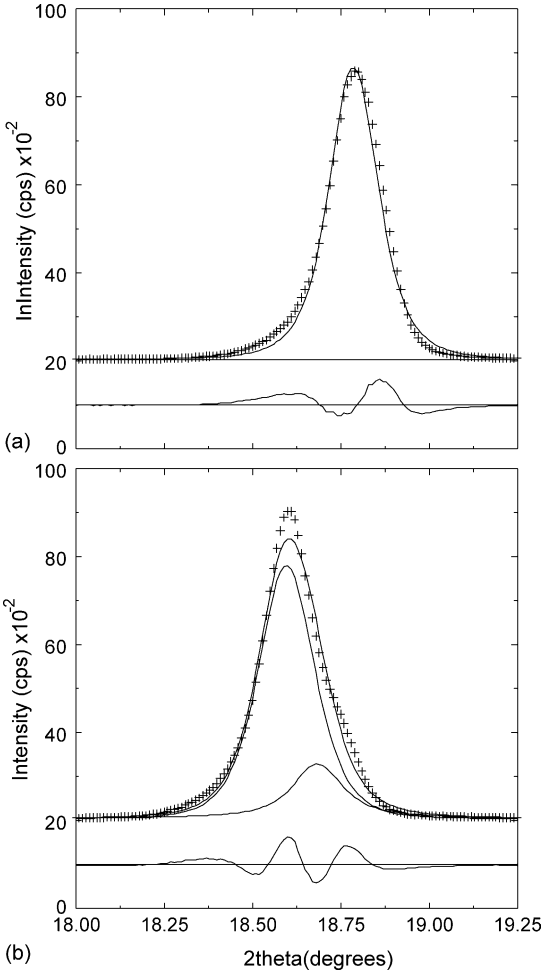

Fig. 5. (0 0 3) XRD profiles for fresh cathode (a) before and (b) after rapid charging.

is charged, this peak moves to a lower angle. Following the rapid charge and immediate removal from the electrolyte, the primary phase present is charged to about $x = 0.12$. A small amount of a second phase (ca. 30% of the total) with $x \sim 0.03$ is also present as a shoulder on the main peak, which has a similar line-width to that of the fresh electrode, indicating a homogeneous distribution of charge within the primary phase. The presence of a second phase with a lower state of charge in this rapidly charged electrode may be due to the lower rate capability of larger particles, resulting in an internal lithium concentration gradient that upon equilibration in the absence of electrolyte produces particles with a lower average state of charge than that of the smaller particles.

The behavior of an air-exposed electrode is strikingly different, even when it is charged slowly. After charging at 62 μA cm^{-2} (*C*/20) for 6 h ($x = 0.18$), relaxing at open circuit for 1 h, and standing after washing and drying for 24 h, there are two very different phases present (Fig. 6a). One is at a higher state of charge ($x = 0.29$) and represents about 57% of the active material. The rest is essentially unchanged from its initial state before charging (Fig. 2). The line-widths of diffraction peaks due to the charged phase are significantly broader than those of the uncharged phase, presumably because there is a range of states of charge present. This is clear from a pattern taken 7 days later (Fig. 6b). The profile of the charged phase has become sharper as the distribution of charge has become more uniform. The average state of charge for this phase has decreased slightly, and it represents a somewhat larger fraction of the active material. The amount of uncharged phase has decreased by a similar amount, but its state of charge has increased only slightly. Li_2CO_3 is still present in both patterns, but at a reduced level relative to that in the uncharged electrode.

This bimodal behavior is strong evidence for isolation of $LiNi_{0.8}Co_{0.15}Al_{0.05}O_2$ particles by some mechanism associated with the formation of Li_2CO_3. The isolated particles are not charged even at a low rate and remain nearly unaffected by the presence of charged particles in the electrode (we can estimate from the charge–discharge curves a driving force for equilibration of the two phases of at least 300 mV). Particle isolation may result from a variety of causes, including: (1) electronic disconnection due to the presence of an insulating coating or to physical separation of particles from the conducting matrix as a result of growth of an insoluble phase; (2) blocking of ions due to the presence of a surface layer with low ionic conductivity; or (3) obstruction of electrolyte transport by an accumulation of insoluble material in pores. Li_2CO_3 has no electronic conductivity, and its lithium ion conductivity is estimated by extrapolation from high temperature data [15,16] to be about 10^{-9} S cm^{-1}.

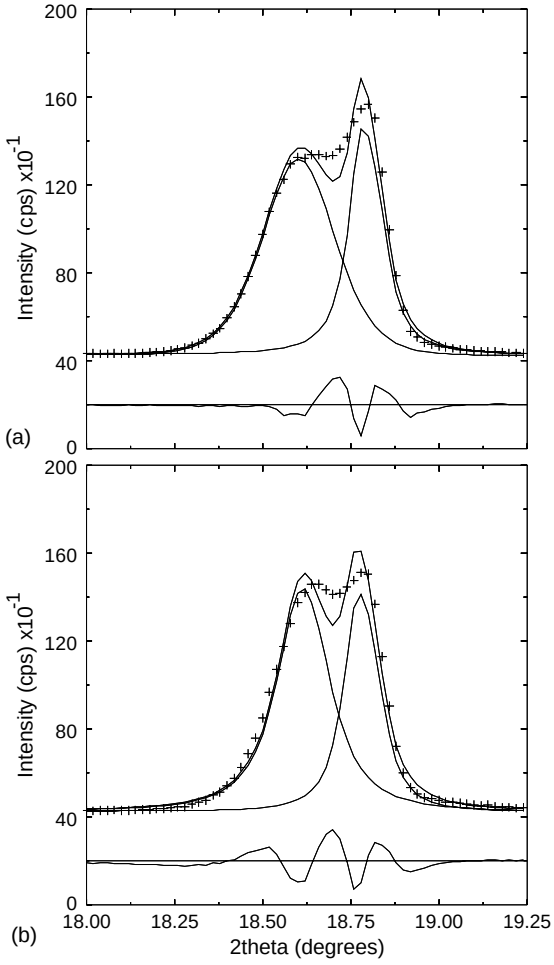

Fig. 6. (0 0 3) XRD profiles for an air-exposed cathode (a) after a low rate charge and (b) after 7 days.

Although an electronic or ionic barrier would increase the impedance of the cathode, it is not clear that such a mechanism would give rise to a bimodal distribution of connected vs. disconnected particles as opposed to a continuous range of more or less isolated grains. The observed bimodal effect could result from physical separation of particles from the conducting matrix (or from the current collector) or from blocking access to a sufficient number of pores to isolate particles from the electrolyte. The latter could be the result of pore clogging through accumulation of Li_2CO_3 deposits or of gas bubble formation due to interaction of acid species with the carbonate.

Particle isolation contributes to both capacity and power losses by disconnecting active material from the system. The remaining (connected) material is charged and discharged at a higher effective rate. The isolation mechanism also may contribute to increased impedance in the connected portions of the electrode. Future work will seek to clarify the mechanism and the role of surface films and reaction byproducts in performance degradation during cycling and storage of high-power lithium ion cells.

4. Conclusions

A thick surface coating formed on $LiNi_{0.8}Co_{0.15}Al_{0.05}O_2$ particles due to prolonged air exposure was shown to consist of lithium carbonate. This coating appears to have been formed by reaction of atmospheric carbon dioxide with lithium oxide residue in the powder and/or by reaction with Li from the $LiNi_{0.8}Co_{0.15}Al_{0.05}O_2$ active material. It produces severe deleterious effects on the capacity and power characteristics of cathodes in lithium cells. An ex situ XRD study showed a distinct bimodal charge distribution in heavily contaminated cathodes which relaxes very slowly. Particle isolation due to Li_2CO_3 formation on the surface of the active material is proposed as the mechanism for power and capacity losses relative to fresh electrodes.

Acknowledgements

The authors acknowledge valuable contributions from Ms. Azucena Sierra, Dr. Seung-Wan Song and Dr. Kathryn Striebel. This work was supported by the Assistant Secretary for Energy Efficiency and Renewable Energy, Office of FreedomCAR and Vehicle Technologies of the US Department of Energy under Contract No. DE-AC03-76SF00098.

References

[1] T. Ohzuku, A. Ueda, M. Nagayama, Y. Iwakoshi, H. Komori, Electrochim. Acta 38 (1993) 1159.
[2] J.G. Chen, B.D. Devries, J.T. Lewandowski, R.B. Hall, Catal. Lett. 23 (1994) 25.
[3] T. Nohma, H. Kurokawa, M. Uehara, M. Takahashi, K. Nishio, T. Saito, J. Power Sour. 54 (1995) 522.
[4] C.-C. Chang, N. Scarr, P.N. Kumta, Solid State Ionics 112 (1998) 329.
[5] G.T.-K. Fey, Z.-X. Weng, J.-G. Chen, T.P. Kumar, Mater. Chem. Phys. 82 (2003) 5.
[6] K. Matsumoto, R. Kuzuo, K. Takeya, Yamanaka, J. Power Sour. 81/82 (1999) 558.
[7] D. Aurbach, K. Gamolsky, B. Markovsky, G. Salitra, Y. Gofer, U. Heider, R. Oesten, M. Schmidt, J. Electrochem. Soc. 147 (2000) 1322.
[8] A.M. Andersson, D.P. Abraham, R. Haasch, S. MacLaren, J. Liu, K. Amine, J. Electrochem. Soc. 149 (2002) A1358.
[9] J.C. Badot, V. Bianchi, N. Baffier, N. Belhadj-Tahar, J. Phys. Condens. Matter 14 (2002) 6917.
[10] H.-K. Kim, T.-Y. Seong, W. Cho, Y.S. Yoon, J. Power Sour. 109 (2002) 178.
[11] R.B. Wright, J.P. Christophersen, C.G. Motloch, J.R. Belt, C.D. Ho, V.S. Battaglia, J.A. Barnes, T.Q. Duong, R.A. Satula, J. Power Sour. 119 (2003) 865.
[12] D. Aurbach, J. Power Sour. 89 (2000) 206.
[13] S.-W. Song, G.V. Zhuang, P.N. Ross, in: Proceedings of the 204th Meeting of The Electrochemical Society, Abstract No. 410, Orlando, FL, October 12–16, 2003.
[14] J. Shim, R. Kostecki, T. Richardson, X. Song, K. Striebel, J. Power Sour. 112 (2002) 222.
[15] J. Mizusaki, H. Tagawa, K. Saito, K. Uchida, M. Tezuka, Solid State Ionics 53/56 (1992) 791.
[16] S. Rama Rao, C.S. Sunandana, J. Phys. Chem. Solids 3 (1996) 315.